HHS Public Access

Author manuscript

Brain Pathol. Author manuscript; available in PMC 2015 July 13.

Published in final edited form as:

Brain Pathol. 2012 January ; 22(1): 41–57. doi:10.1111/j.1750-3639.2011.00501.x.

Aberrant Upregulation of Astroglial Ceramide Potentiates Oligodendrocyte Injury

SunJa Kim[a], **Andrew J. Steelman**[a], **Yumin Zhang**[b], **Hannah C. Kinney**[c], and **Jianrong Li**[a,1]

[a]Department of Veterinary Integrative Biosciences, Texas A&M University, College Station, TX 77843

[b]Department of Anatomy, Physiology and Genetics, Uniformed Services University of the Health Sciences, Bethesda, MD 20814

[c]Department of Pathology, Children's Hospital Boston and Harvard Medical School, Boston, MA 02115

Abstract

Oligodendroglial injury is a pathological hallmark of many human white matter diseases, including multiple sclerosis and periventricular leukomalacia. Critical regulatory mechanisms of oligodendroglia destruction, however, remain incompletely understood. Ceramide, a bioactive sphingolipid pivotal to sphingolipid metabolism pathways, regulates cell death in response to diverse stimuli and has been implicated in neurodegenerative disorders. We report here that ceramide accumulates in reactive astrocytes in active lesions of multiple sclerosis and periventricular leukomalacia, as well as in animal models of demyelination. Serine palmitoyltransferase, the rate-limiting enzyme for ceramide *de novo* biosynthesis, was consistently upregulated in reactive astrocytes in the cuprizone mouse model of demyelination. Mass spectrometry confirmed the upregulation of specific ceramides during demyelination and revealed a concomitant increase of sphingosine as well as a suppression of sphingosine-1-phosphate, a potent signaling molecule with key roles in cell survival and mitogenesis. Importantly, this altered sphingolipid metabolism during demyelination was restored upon active remyelination. In culture, ceramide acted synergistically with tumor necrosis factor leading to apoptotic death of oligodendroglia in an astrocyte-dependent manner. Taken together, our findings implicate that disturbed sphingolipid pathways in reactive astrocytes may indirectly contribute to oligodendroglial injury in cerebral white matter disorders.

Introduction

Oligodendrocytes (OLs) are essential for the function of the vertebrate central nervous system (CNS) by forming myelin that enables saltatory conduction of nerve impulses. Myelination is a highly regulated multi-step process that occurs in the human CNS primarily in late prenatal and early postnatal life (9, 36). Disruption of OL lineage progression and interaction with axons, or damage to myelin/OLs underlies many human neurological

[1] Corresponding author: Jianrong Li, Ph.D., Department of Veterinary Integrative Biosciences, Texas A&M University, Mail Stop 4458, College Station, TX 77843, Phone: 979-862-7155, Fax: 979-847-8981, jrli@cvm.tamu.edu.

disorders including multiple sclerosis (MS) and periventricular leukomalacia (PVL). Multiple sclerosis is the most common inflammatory demyelinating disease of the CNS, and is pathologically characterized by inflammatory cell infiltration, OL death, demyelination, axonal damage and gliosis (39, 57). In relapses and remitting MS, certain levels of remyelination occur but this spontaneous repair capability diminishes over time (18). Periventricular leukomalacia, on the other hand, is the principal injury of the perinatal brain that underlies cerebral palsy and cognitive deficits associated with prematurity (60). Pathologically, it is characterized by premyelinating OL injury, hypomyelination, focal periventricular necrosis, and diffuse gliosis and microglial activation in the immature cerebral white matter. In both entities, reactive astrocytes have long been recognized as a cellular feature of the pathology but have been largely ignored on their potential contributions to OL damage. In the present study, we sought to determine if ceramides, which we show here for the first time accumulate in reactive astrocytes in both disorders, play a role in oligodendroglial injury.

Specific sphingolipid metabolites such as ceramide, sphinogosine (Sph) and sphingosine-1-phosphate (S1P) have emerged as a new class of bioactive lipids that functions as second messengers by binding to specific intracellular targets (17, 22, 37). They also function as signaling molecules capable of acting in a paracrine manner, regulating cell growth, differentiation, survival, migration and immune responses. Ceramide is at the center of interconnected metabolic pathways of sphingolipids (Figure S1), and is synthesized *de novo* from serine and palmitoyl CoA or produced from sphingomyelinase (SMase)-catalyzed degradation of sphingomyelin. Breakdown of ceramide via ceramidase (CDase) produces Sph, which can be phosphorylated to S1P via Sph kinases or recycled back to ceramide. Ceramide is generated in response to diverse stimuli including proinflammatory cytokines, lipopolysaccharide, and oxidative stress, and could potentially act as a shared downstream signaling molecule in cell injury common to many otherwise diverse disorders. Since oligodendroglial damage is a key factor in the pathogenesis of MS and PVL, we examined in this study whether ceramide metabolism is dysregulated using postmortem tissues from MS and PVL patients, as well as in animal models of demyelination and remyelination. We report here that ceramide is aberrantly accumulated in reactive astrocytes and that ceramide potentiates OL damage in an astrocyte-dependent manner. Our data suggest that reactive astrocytes may directly contribute to OL injury.

Materials and Methods

Materials

DMEM, HBSS and GFAP antibody were obtained from Invitrogen (Carlsbad, CA). PDGF and basic FGF were from PeproTech (Rocky Hill, NJ). Antibody against Iba1 was purchased from Wako chemicals (Richmond, VA). Antibodies against Olig2 and 2', 3'-cyclic nucleotide 3'-phosphodiesterase (CNPase) were from Millipore (Billerica, MA). Active caspase-3 antibody was from Cell Signaling (Danvers, MA). CD68 antibody was from Dako (Glostrup, Denmark). Mouse anti-ceramide IgM antibody (MAS0013) was obtained from Glycobiotech GmbH (Küekels, Germany), and mouse anti-ceramide monoclonal IgM antibody (clone MID 15B4) was from Alexis Biochemicals (Plymouth Meeting, PA).

Antibodies against serine palmitoyltransferase (SPT), mouse aCDase and NeuN were from Cayman Chemical (Ann Arbor, MI). Normal mouse IgM was purchased from Jackson ImmunoResearch Lab (West Grove, PA). N-acetylsphingosine (C2-ceramide), N-hexanoyl-D-sphingosine (C6-ceramide) and N-oleoylethanolamine (NOE) were obtained from Sigma (St. Louis, MO). C18-ceramide was purchased from Avanti Polar Lipids (Alabaster, AL). TNF was obtained from R & D Systems (Minneapolis, MN). Unless specified otherwise, all other reagents were from Sigma.

Human tissues and sample preparation

Frozen and formalin fixed brain tissues from patients with clinically diagnosed and neuropathologically confirmed MS and from controls were obtained from the Rocky Mountain MS Center Tissue Bank (Englewood, CO) and the Human Brain and Spinal Fluid Resource Center (Los Angeles, CA). Formalin fixed human PVL and age-related control brain specimens were from archived autopsy cases at Children's Hospital Boston, MA. Frozen tissue specimens were bisected with one-half used for tissue homogenization for sphingolipid analysis and one-half for histology and immunostaining examination upon post-fixation with 4% paraformaldehyde for 1d followed by cyroprotection with 30% sucrose in 0.1M PBS. The fixed tissues were cryosectioned at 10 μm. Tissue homogenization was carried out in 0.05 M phosphate buffer (pH 7.0) containing 10 mM sodium pyrophosphate, 10 mM sodium floride, 1 mM sodium vanadate, 80 μM aprotinin, 104 μM AEBSF, 4 μM Bestatin, 1.4 μM E-64, 2 μM Leupeptin, 1.5 μM Pepstatin A, and 100 μg/ml phenylmethylsulfonyl fluoride.

Mouse models of demyelination

Age-matched C57BL/6 mice were used in two distinct mouse models of demyelination. Mice were housed in standard animal housing facility in accordance with NIH guidelines for Care and Use of Laboratory Animals. Food and water were provided *ad libitum.* Animal protocols were approved by the Texas A&M University (cuprizone model) and the Uniformed Services University of the Health Sciences (EAE model) Institutional Animal Care and Use Committees. Cuprizone-induced demyelination was achieved by feeding 8 wk-old male C57BL/6 mice cuprizone milled into normal chow at a concentration of 0.2% (Harlan) for 5 wk or 3 wk when indicated. At the end of cuprizone feeding, about half of the mice were killed to examine demyelination and the other half were returned to normal diet for an additional 2 weeks to examine remyelination as described (Steelman et al., submitted). Age-matched control mice were kept on normal diet throughout the duration of the cuprizone experiment. EAE was induced in female C57BL/6 mice at between 7-9 week of age with an emulsion injected subcutaneously at two sites, one at each of the hind flanks (0.1 ml/site). The injections to the hind flanks yielded a total of 200 μg myelin oligodendrocyte glycoprotein (MOG; NeoMPS, San Diego, California) peptide 35-55 in complete Freund's adjuvant (CFA; DIFCO Laboratories, Detroit, MI) with 500 μg *mycobacterium tuberculosis* (DIFCO). Control mice (sham) were injected with CFA without the MOG peptide. Immediately following CFA injections, and 24 hours later, mice were injected intraperitoneally with 200 ng of inactivated *pertussis toxin* (List Biologicals, Campbell, CA). One week after induction of EAE mice received a booster of MOG peptide in Incomplete Freunds Adjuvant (IFA) and control mice were injected with IFA without the

MOG peptide. Animals were scored for clinical signs from day 10 onward and neurological signs were assessed as: 0, normal; 1, piloerection, tail weakness; 2, tail paralysis; 3, tail paralysis plus hindlimb weakness/paralysis; 4, tail, hind and fore limb paralysis; and 5, moribund/dead, using increments of 0.5 points for intermediate clinical findings (32). Animals (n=3 per group) were killed 2 wk after EAE induction and all received clinical score of 2.

Primary cell cultures

Primary OLs, astrocytes, and mixed glial cultures were prepared from forebrains of 1- to 2-d-old Sprague-Dawley rat pups as described previously (40, 41). Briefly, forebrains free of meninges were dissociated and plated onto poly-D-lysine-coated T75 flasks or directly into 24-well plates for experiments using mixed glia and fed every other day for 7–10 d. The flasks were pre-shaken for 1 h at 200 rpm to remove lightly attached microglia followed by overnight shaking to separate OLs from the astrocyte layer. Isolated OLs were plated either by themselves or onto poly-dl-ornithine (PO)-coated 24-well plates containing established astrocytes for co-cultures. Cells were maintained in a serum-free basal defined medium (BDM) (DMEM with 0.1% bovine serum albumin, 50 μg/ml human apo-transferrin, 50 μg/ml insulin, 30 nM sodium selenite, 10 nM D-biotin, and 10 nM hydrocortisone) containing 10 ng/ml PDGF-AA and 10 ng/ml basic FGF for 5–9 d. In OL monocultures, contamination of astrocytes and microglia was <2%. Astrocytes were purified (>95%) from the astrocyte layer in the flask after being exposed to a specific microglia toxin L-leucine methyl ester (1 mM) for 1 h and were subcultured 1-2 times. For regular astrocyte and OL co-cultures, astrocytes (2.4×10^5 cells per well) were plated into 24-well culture plates 1~2 days before seeding OLs (6×10^4 cells per well), and the co-cultures were used within 2-3 days. For bridged, no cell contact co-cultures of astrocytes and OLs, OLs were cultured on PO-coated coverslips on which 1mm tall PDMS mini-columns were attached at 4 corners as described (35). The coverslips were then transferred to 24-wells containing astrocytes.

Cell treatment and survival determination

Cells were treated in triplicate with C2-, C6-, C18-ceramide, or the ceramidase inhibitor NOE in the presence or absence of TNF as specified in figure legends. OL survival was analyzed 40–48 h later by immunocytochemistry and counting of $O4^+$ cells with normal nuclei as described earlier (41). Total number of cells was revealed by staining all nuclei with bisbenzimide. Five-ten random consecutive fields were counted in each coverslip under 200x magnification with a total of >1000 cells counted in the control conditions. Cell survival is expressed as mean ± SEM.

Mouse tissue preparation for immunohistology analyses

Mice were anesthetized and intracardially perfused with PBS followed by 4% paraformaldehyde. Brains (cuprizone mice) and spinal cords (EAE mice) were dissected out, post-fixed in 4% paraformaldehyde overnight at 4°C and cryoprotected in 30% sucrose until sunk. The fixed tissue was embedded in Tissue Tek OCT (Sakura, Torrance, CA) and stored at −80°C. Sagittal or coronal sections of mouse brains or transverse sections of lumbar spinal cords were cut at 20 and 14 μm, respectively, and mounted onto Superfrost Plus slides for immunohistochemical analysis.

Mouse brain sample preparation for RNA, protein and lipid extraction

Mice were transcardially perfused with 20ml of sterile PBS. The brain was removed, and the corpus callosum as well as portion of cingulate gyrus, external capsule and striatum was quickly but meticulously dissected using a sterile razor blade. Each piece of tissue was flash frozen in liquid nitrogen and stored at −80°C. The dissected brain regions were used for quantitative RT-PCR (qRT-PCR), western blotting analysis, and sphingolipid quantification.

Quantification of endogenous sphingolipids by mass spectrometry

Human autopsy tissues and dissected animal brain tissues were homogenized. An equal amount of tissue homogenate (1mg proteins/sample) was fortified with internal standards, extracted with ethyl acetate/isopropanol/water (60:30:10, v/v/v), and analyzed by a High-Performance Liquid Chromatography–Tandem Mass Spectrometry (HPLC-MS/MS) system at the Lipidomics Shared Resource Center at Medical University of South Carolina as detailed previously (8). Quantitative analysis of sphingolipids was based on calibration curves generated by spiking an artificial matrix with known amounts of target analytes and standards. Specific sphingolipid levels were normalized based on the level of total phospholipids in human samples or the amount of proteins in animal samples. Total phospholipids were determined using EnzyChrome™ Phospholipid assay Kit (BioAssay Systems, Harward, CA).

Quantitative RT-PCR analysis of nSMase and aSMase expression

qRT-PCR was used to determine the effects of cuprizone on nSMase and aSMase transcripts in the CNS. Briefly, RNA was extracted with TRI reagent (Sigma), quantified by NanoDrop 1000 spectrophotometer (ThermoFisher Scientific, Rockford, IL), treated with DNase I (Invitrogen), and reverse transcribed using a Promega AMV-reverse transcriptase kit and random oligonucleotide primers. Specific cDNAs were amplified and analyzed using a 7500 Real Time PCR System (Applied Biosciences). Primers used were nSMase, forward-GAGTTCCACGTCTGCTGTGA, reverse-TTAGCACGCTGATCAAATCG; aSMase, forward- TTCCCGAGTGCTGCTTATCT, reverse-CTATCCAGAGCACTGAGCCC; and β-actin, forward-AGACTTCGAGCAGGAGATGG, reverse-CCATCATGAAGTGTGACGTTG. All samples were run in duplicate or triplicate, and gene expression was normalized to β-actin and fold expression was calculated using the formula $2^{-\Delta\Delta Ct}$.

SMase activity assay

Activity of SMases was measured using the Amplex (10-acetyl-3,7-dihydroxyphenoxazine)-Red Sphingomyelinase Assay Kit (Molecular Probes, Carlsbad, CA). Brain tissue extracts prepared as above were diluted in lysis buffer (0.05 M phosphate buffer, pH 7.0, 0.1% Triton X-100, 80 μM aprotinin, 104 μM AEBSF, 4 μM bestatin, 1.4 μM E-64, 2 μM leupeptin, 1.5 μM pepstatin A, and 100 μg/ml phenylmethylsulfonyl fluoride) and incubated on ice for 30 min. After centrifugation at 17,000 ×g for 15 min, supernatants were collected, and protein concentrations were determined using BioRad DC protein assay reagents. 100 μl of each sample (400 μg proteins) was added to a 100 μl assay mixture containing 100 μM Amplex Red reagent, 2 u/ml horseradish peroxidase, 0.2 u/ml choline oxidase, 8 u/ml

alkaline phosphatase, and 0.5mM sphingomyelin in reaction buffer (0.1 M Tris-HCl, 10 mM MgCl2, pH 7.4). After 30 min incubation in dark at 37°C, the fluorescence was measured with a plate reader (FluoStar Optima, BMG Labtech Inc, Offenburg, Germany) using excitation λ=544 nm and emission λ=590 nm. The values were corrected from background signal determined by omitting tissue extracts.

For acid SMase activity measurement, tissue extracts were diluted in acidic buffer solution (final concentrations, 50 mM sodium acetate, pH 5.0, 0.1% Triton X-100, 1 μg/ml aprotinin, 1 mM EDTA, and 100 μg/ml phenylmethylsulfonyl fluoride) and incubated on ice for 30 min. Acid SMase activity was then assayed by a two-step reaction system. First, to generate phosphocholine and ceramide, 0.5 mM sphingomyelin was added to the samples and incubated for 60 min at 37°C. Next, the reaction was placed on ice and 100 μl of 100 μM Amplex Red reagent, 2 u/ml horseradish peroxidase, 0.2 u/ml choline oxidase and 8 u/ml of alkaline phosphatase in reaction buffer (0.1 M Tris-HCl, pH 8.0) was added. The samples were further incubated for 30 min at 37°C and the fluorescence was determined as above.

Immunohistochemistry, TUNEL, and immunofluorescence microscopy

For paraffin-imbedded tissue sections, antigen retrieval was carried out by autoclaving the tissue sections for 20 min in sodium citrate buffer (10 mM sodium citrate, 0.05% Tween20, pH 6.0) after deparaffinization. For frozen tissue sections, no antigen retrieval was needed. Tissue sections were rinsed with TBS (50 mM Tris-HCl, pH 7.4, 150 mM NaCl) and blocked with TBS-T (0.1% Triton X-100) containing 5% goat serum for 1 hr at room temperature. Sections were then incubated overnight at 4°C with antibodies against Iba1 (1:2000), GFAP (1:1000), active caspase-3 (1:1000), CNPase (1:100), human CD68 (1:100), mouse SPT (1:100), ceramide (monoclonal IgM, MID15B4, 1:50), or ceramide (mouse IgM, MAB0013, 1:50), or normal mouse IgM (4 μg/ml). For colormetric detection of specific immunolabeling, the Vectastain ABC kit (Vector Laboratories, Burlingame, CA) was used. For immunofluorescence staining, secondary antibodies conjugated with AlexaFluor 488 or AlexaFluor 594 (1:1000; Invitrogen) were used. Nuclei were stained with bisbenzimide as described before (41). Since adult human brain tissue sections exhibited autofluorescence, before mounting the stained tissue sections with FluoroMount, autofluorescence was quenched with 0.5% Sudan black in 70% ethanol. Additionally, because Sudan black stains neutral lipid and myelin, this step allows visualization of immunostaining and myelin in the same sections. In some cases, oil red O was used for detecting myelin. To label fragmented DNA, terminal deoxynucleotidyl transferase-mediated dUTP nick end labeling (TUNEL) was performed using an In Situ Cell Death detection kit (Roche, Indianapolis, IN). All images were captured with a fluorescence microscope equipped with an Olympus DP70 digital camera (model IX71; Olympus, Tokyo, Japan).

Negative controls in which primary antibodies were omitted did not show signals in cuprizone, EAE, PVL and MS tissue sections. Nor was there significant signal if the ceramide primary antibodies were replaced with normal mouse IgM antibodies. To semi-quantify ceramide immunoreactivity in human brain sections, multiple fluorescence images were taken from 3 different regions of cerebral white matter for each case using same image acquisition settings including exposure times. For control cases, images were taken from

random regions of the white matter. For MS samples, images were taken from lesion-surrounding areas. Relative fluorescence intensity was then visually scored in a blinded fashion by two independent investigators, and the scores were consistent with that calculated using the Image J software (U. S. National Institutes of Health, Bethesda, MD, http://rsb.info.nih.gov/ij). Ceramide immunoreactivity was classified qualitatively and semi-quantitatively by two independent investigators as follows: −, minimal signal; +, weak-moderate; ++, moderate-strong; and +++, strong based on fluorescence intensity and the density of ceramide-positive cells.

Western blot analysis

Tissue homogenates were separated by 10-15% SDS-PAGE and transferred to PVDF membranes. The membranes were blocked with 5% non-fat milk or bovine serum albumin in TBS-T (0.1% Tween 20) for 1 h and then incubated with primary antibodies against SPT (1:2000) and aCDase (1:500) overnight at 4°C. Following washings, the membranes were incubated with HRP-conjugated secondary antibody and immunoreactive bands were visualized by chemiluminescence using SuperSignal detection reagents (ThermoFisher Scientific). Western blot images were acquired using Molecular Imager ChemiDoc XRS+ System (Bio-Rad, Hercules, CA) and in some cases specific bands were quantified using the QuantityOne software and normalized against β-actin.

Statistical analysis

Data were expressed as mean ± SEM and analyzed by one-way ANOVA followed by Bonferroni's *post hoc* test to determine statistical significance. Comparison between two experimental groups was based on two-tailed *t* test. We considered $p<0.05$ as statistically significant.

Results

Ceramide is aberrantly accumulated in reactive astrocytes around/in actively demyelinating lesions in MS and in animal models of demyelination

We and others have demonstrated that premyelinating OLs and mature OLs are variably susceptible to injury induced by diverse stimuli such as proinflammatory cytokines and reactive oxygen/nitrogen species and to excitotoxicity (10, 24). Since intracellular ceramide can also be produced in response to diverse stimuli and is well documented for its capability to directly induce cell death (30), we reasoned that elevated ceramide may represent a common signal mediating OL injury. Interestingly, in actively demyelinating MS lesions, as judged by myelin breakdown and active phagocytosis of myelin debris by macrophages (Figure 1A-C), specific ceramide immunoreactivity was observed in $GFAP^+$ reactive astrocytes in and around the boarder of demyelinating plaques (Figure 1A, D, E, J), but not in normal-appearing white matter (Figure 1K) or in the white matter from controls (not shown). The ceramide immunoreactivity was confined to astrocytes, exhibited punctuate staining patterns, and did not co-localize to activated microglia/macrophages (Figure 1F-H). Staining of adjacent serial tissue sections with an IgM isotype control antibody did not reveal any labeling (Figure 1I). Two specific anti-ceramide antibodies that have been demonstrated by others to be specific for endogenous ceramide (14, 19, 49, 59, 61) were

used. Both antibodies showed similar staining patterns in the cerebral white matter, and labeled reactive astrocytes in the lesions (Figure S2). Of note, ceramide immunoreactivity was also found in some blood vessels (Figure S2). Importantly, $TUNEL^+$ cells were observed around the demyelinating lesion edge where $ceramide^+$ astrocytes were also prominent in adjacent serial sections (Figure 1L). The $TUNEL^+$ cells expressed OL marker CNPase, indicating damaged OLs in demyelinating lesions (Figure 1M).

Immunohistological analysis of 8 control and 13 MS cases revealed ceramide immunoreactivity in reactive astrocytes in 10 MS cases (Table 1). Due to the known heterogeneity of MS neuropathology (43), we next examined the above findings using two well-established animal models of demyelination. Experimental autoimmune encephalomyelitis (EAE) is a T cell-mediated disease of the CNS with inflammatory demyelinating lesions similar to type I and II MS lesions (43, 56). In contrast, cuprizone intoxication of rodents results in OL apoptosis, prominent gliosis, and demyelination of specific cerebral white matter regions (*e.g.*, corpus callosum) independent of T cells (44, 46), features observed in type III and IV MS lesions (43, 49, 56). We found that ceramide immunoreactivity was indeed markedly upregulated in astrocytes but not microglia/macrophages in demyelinating lesions in EAE mice (Figure 2A-C) and in the caudal corpus callosum of cuprizone-fed mice (Figure 2D-H). OLs in demyelinating cerebral white matter did not appear to accumulate ceramide, as determined by double immunohistochemistry for ceramide and Olig2, a transcription factor of oligodendroglial lineage cells (Figure 2I). Other OL markers such as CC1 and CNPase were not used for double labeling with ceramide because the antibodies were all generated from mice. Five week cuprizone feeding caused reproducible demyelination in multiple specific brain regions in addition to the corpus callosum. In all demyelinating regions examined including cerebellum, cortex, and hippocampus, but not in controls, we found ceramide accumulation in reactive astrocytes (Figure S3). Consistent with these observations, increased ceramide production in astrocytes was also observed in mice intoxicated for 3 weeks (Figure S4), when OL apoptosis peaked in the corpus callosum (46) (data not shown). Taken together, our results demonstrate aberrant upregulation of ceramide in reactive astrocytes during demyelination in MS and in animal models of MS.

Accumulation of ceramide in human PVL

To determine whether astroglial accumulation of ceramide during demyelination of the adult CNS also occurs in white matter injury during development when myelin is not yet formed, we examined human PVL cases and controls related in age (Table 2). Since diffuse gliosis is most pronounced surrounding foci of periventricular necrosis in PVL (25, 26), we focused on diffuse gliosis in our analysis of human PVL. Distinct and punctate ceramide staining was found within reactive astrocytes in the diffusely gliotic component of the deep white matter region (Figure 3C), whereas minimum immunolabeling was observed at the level of the subcortical white matter (Figure 3B). There appears to be a close spatial relationship between activated microglia/macrophages and ceramide-positive astrocytes across the cerebral white matter region (Figure S5).

Disrupted sphingolipid metabolism during demyelination

To confirm the above results, we then used lipid chromatography tandem mass spectrometry to determine and quantify simultaneously specific ceramide species and other sphingolipid metabolites from tissue extracts (8). C18:0 ceramide was found to be significantly elevated in MS samples when compared to controls (Figure 4A). While there appeared to be increases in C18:1, C24:0 and C24:1 ceramide levels in MS, the elevation was not statistically significant. Levels of Sph and S1P also showed variations among these human autopsy samples and were not statistically significant (Figure 4B). It should be noted that a recent study reported a decreased level of S1P and increased ratio of C16 or C18 over C24 in MS lesions, albeit the level of statistical significance was not provided (53).

Because of the heterogeneity of human postmortem samples, we decided to employ the cuprizone mouse model of demyelination to investigate further alterations of sphingolipid metabolism during demyelination. We chose the cuprizone model for these analyses largely because the toxin-induced OL death and demyelination occur reproducibly in well-defined anatomical areas in the brain, and are independent of peripheral lymphocytes, enabling direct analysis of sphingolipid metabolism within the CNS parenchyma without the complication from activated lymphocytes. Consistent with the immunohistochemical findings, we found significantly elevated levels of C16:0, C18:0, C20:0, dihydroC16 (dhC16) ceramides and Sph, and diminished levels of dihydroS1P (dhS1P) and S1P in the white matter of cuprizone-fed mice (Figure 4C, D). As the relative balance of ceramide and S1P is an important determinant for cell death and survival (55), this inverse relationship between ceramide and S1P/dhS1P during demyelination suggests a role for sphingolipids in regulating oligodendroglial cell demise.

Serine palmitoyltransferase, the rate-limiting enzyme for ceramide biosynthesis, is upregulated in reactive astrocytes in the corpus callosum of cuprizone-fed mice

The level of intracellular ceramide is maintained by interconnected metabolic pathways that are localized in various subcellular compartments and are under different regulation (22). To explore whether the increased levels of astroglial ceramide in demyelinating regions was a result of increased sphingolipid metabolism, we examined enzymes involved in ceramide biosynthesis (sphingomyelin breakdown and *de novo* synthesis) and ceramide degradation. Expression and enzymatic activity of neural SMase (nSMase) and acid SMase (aSMase) were not altered in cuprizone-fed mice when compared to controls, with aSMase accounting for the majority of SMase activity in the brain (Figure 5A, B). Similarly, acid ceramidase (aCDase) expression was not significantly different between control and cuprizone-fed mice (Figure 5C). In contrast, while serine palmitoyltransferase (SPT) was essentially absent in the corpus callosum of control mice (Figure 5D), it was markedly upregulated in reactive astrocytes in the caudal region of the corpus callosum where demyelination occurs (Figure 5E-F) and where the ceramide-positive astrocytes were observed (Figure 2 and Figure 5F). Furthermore, SPT^{+} astrocytes in the caudal corpus callosum were also immunereactive for ceramide (Figure 5H). It is noteworthy that neurons endogenously expressed high level of SPT (Figure 5G). The fact that SPT is upregulated in reactive astrocytes that also accumulate ceramide suggests a potential involvement of the *de novo* ceramide synthesis

pathway. This is in agreement with our findings on alterations of metabolites of the *de novo* pathway such as dhC16 as well as dhS1P in cuprizone-fed mice (Figure 4D).

Ceramide acts synergistically with TNF to induce apoptotic death of OLs in an astrocyte cell contact-dependent manner

To explore the functional consequence of astroglial accumulation of ceramides to OLs, we next employed an *in vitro* model for cytokine-mediated toxicity toward oligodendroglia (41). We treated mixed glial cultures with cell permeable C2 ceramide at concentrations not directly toxic to cells and then examined OL survival. We found that ceramide acted synergistically with low dose of TNF, resulting in significant loss of OLs (Figure 6A, B). Interestingly, this synergism between ceramide and TNF was completely lost in OL monocultures (Figure 6C), indicating a non-cell autonomous effect. Consistent with these results, in co-cultures of astrocytes and OLs, C2, C6 and the long chain C18 ceramides all caused significant oligodendroglial death in the presence of low levels of TNF (Figure 7A). Furthermore, increasing endogenous ceramides via blocking ceramide degradation with ceramidase inhibitor N-oleoylethanolamine (NOE) similarly potentiated TNF toxicity (Figure 7A). Under these conditions, oligodendroglial cells underwent a caspase-dependent apoptotic cell death, as demonstrated by TUNEL labeling of DNA fragmentation (Figure 7B, C), caspase-3 activation in dying oligodendroglial cells in ceramide/TNF-treated co-cultures (Figure 7D-F), and by blockade of the cell death with zVAD-fmk, a pan-caspase inhibitor (Figure 7G). Interestingly, ceramide and TNF failed to induce cell death if astrocytes and OLs were co-cultured in two separate layers distanced at 1mm without direct cell-cell contact (Figure 7H). To further determine whether the synergism between ceramide and TNF is due to a direct effect on astrocytes, we pretreated astrocytes with ceramide, TNF, or ceramide plus TNF for 24 hr followed by extensive washes before plating OLs into the pretreated astrocyte cultures. We found that astrocytes pretreated with ceramide plus TNF were subsequently toxic to added OLs (Figure 7I), albeit to a less degree as compared to those of co-cultures (Figure 7A). Taken together, these results demonstrate that ceramide and TNF synergistically induce oligodendroglial cell death via a mechanism dependent on astrocytes. The data also agree with our immunohistological observation of co-existence of ceramide-laden astrocytes and $TUNEL^+$ OLs around actively demyelinating lesions in some MS cases (Figure 1).

Elevation of astroglial ceramide and depletion of S1P during CNS demyelination are reversed during remyelination

The fact that astrocytes accumulate ceramide in association with cuprizone-induced OL damage and demyelination, and that ceramide sensitizes OLs to TNF toxicity in co-cultures of astrocytes and OLs suggests a potential pathological role for astrocytes in demyelination. Since the cuprizone model provides a unique opportunity to study signals involved in CNS remyelination processes without the complication of adaptive immune responses, we sought to determine ceramide metabolism during the remyelinating process. As mentioned, cuprizone intoxication for 3 weeks caused OL apoptosis and significant increases of C16:0/C18:0 ceramides and suppression of dhS1P/S1P (Figure S4D). Mice intoxicated for 5 weeks were severely demyelinated in the caudal corpus callosum (Steelman et al, submitted). Cessation of cuprizone was followed by a spontaneous repair process and remyelination

(46). Two weeks after cuprizone withdrawal, more than one third demyelinated axons underwent active remyelination as determined by transmission electron microscopy (Steelman et al, submitted). Increased levels of Sph and C16:0, C18:0, and C20:0 ceramides during demyelination were either returned to control levels or significantly decreased during the active remyelinating phase (Figure 8). Concomitantly, S1P and dhS1P, which were depleted during demyelination, returned to the normal level during the remyelinating process (Figure 8). The results thus reveal a close relationship between altered bioactive sphingolipid metabolites and demyelination/remyelination, and suggest a potential of modulating the ceramide/S1P pathway in promoting myelin repair.

Discussion

Bioactive sphingolipid metabolites such as ceramide, Sph and S1P mediate multiple biological functions and have recently received increasing attention as potential therapeutic targets for diverse disease conditions ranging from cancer to atherosclerosis, inflammation, and autoimmune disorders such as MS. In this study, we report that ceramides are aberrantly accumulated in reactive astrocytes in actively demyelinating MS lesions, in diffuse lesions of PVL, and in animal models of demyelination. Ceramides such as C16:0, C18:0 and C20:0 are significantly increased and are associated with a concomitant decrease in S1P levels during demyelination in the cuprizone model of demyelination. In culture, ceramides act synergistically with TNF to induce apoptotic death of OLs via an astrocyte contact-dependent mechanism. Furthermore, we found that elevated astroglial ceramide during cuprizone-induced demyelination is restored during active remyelination in conjunction with an increase in tissue level of S1P. Our results imply that the relative levels of ceramide and S1P may determine OL cell demise.

Astrocyte dysfunction has been linked to a variety of neurological disorders (7, 28) including MS (5, 33). Over-production of endogenous retrovirus glycoprotein syncytin or transmembrane TNF in astrocytes results in neuroinflammation and demyelination (1, 4, 5). Our current findings indicate that elevated astroglial ceramides potentiate OL injury as ceramide markedly synergizes TNF toxicity in an astrocyte contact-dependent manner, a finding consistent with our previous reports (35, 41). It is plausible that aberrant accumulation of ceramides leads to dysfunctional astrocytes that subsequently contribute to OL injury. Alternatively, ceramides or their bioactive derivatives released from reactive astrocytes may directly impact on OLs and promote apoptotic cell death. In fact, exogenous ceramide appears to preferentially kill OLs when compared to astrocytes and neurons (11, 54). While the etiology and age predilection of MS and PVL vary considerably (*e.g.*, adults in the former versus preterm neonates in the latter), these two disorders share pathologic features of activation of astrocytes and microglia, production of inflammatory cytokines, and damage to OL lineage cells. We speculate that astroglial accumulation of ceramides may represent a stress response to pathological mediators. Indeed, increased ceramide levels have been reported in Alzheimer's disease (15, 21), HIV-induced dementia (23, 50), amyotrophic lateral sclerosis (16), and hypoxia/ischemia (52). It is noteworthy that prominent ceramide immunoreactivity was also observed in microvessels in the cerebral white matter of PVL and MS (Figure S2, S5C). Ceramide and its metabolites have been previously implicated in modulating vascular functions including vascular tones and integrity (2, 42).

Cellular levels of ceramide are tightly regulated by complex and interconnected pathways in various subcellular locations. Disruption of one particular sphingolipid metabolic pathway may compromise the other. The importance of a balanced sphingolipid metabolism is underscored by human diseases resulting from genetic defects in the metabolism of sphingolipids, including certain leukodystrophies (38, 62). Interconversion between ceramide and other bioactive sphingolipid species such as Sph and S1P allows perturbation of one potentially influencing the other. Over 2 dozen distinct enzymes can act on ceramide as a substrate or a product, and regulation of many of these enzymes is just beginning to be understood (22). Our finding of SPT upregulation in reactive astrocytes at demyelinating areas in the cuprizone animal model indicates that the *de novo* pathway is most likely to account for the aberrant accumulation of ceramides in these cells. In support of this idea, SPT1 and/or SPT2 have been shown to be upregulated in response to endotoxin and cytokines (47). Furthermore, lipidomics analysis reveals elevated ceramide levels in rat hippocampus after kainate-induced excitotoxic injury (20), in part due to SPT upregulation in reactive astrocytes (27). Whether SPT is upregulated in reactive astrocytes in human MS and PVL tissues remains to be determined since we found that in all control autopsy cases, SPT was endogenously and strongly expressed in astrocytes in the cerebral white matter (Kim and Li, unpublished observation). Thus, future studies are needed to determine the contribution of the *de novo* ceramide synthesis pathway to the white matter injury.

Although the current study cannot exclude the possibility that degradation of myelin sheath may account for elevations of specific ceramides during demyelination, our data do not support this as a main contributor for astroglial accumulation of ceramides. This is based on the fact that (1) aberrant ceramide accumulation also occurs in PVL brain when myelin is not yet developed; and (2) degradation of complex glycosphingolipids occurs primarily in late endosome and lysosomes, producing ceramides that are sequestered in lysosomes and then converted to Sph (12, 52). Accumulation of ceramides through this salvage pathway requires ceramide synthases, key enzymes in the *de novo* pathway. However, we did not detect any ceramide immunoreactive microglia/macrophages in demyelinating MS lesions or in the cuprizone-induced demyelination model, as otherwise expected for these phagocytes. Our data demonstrate that sphingolipid metabolism is disrupted during demyelination. The close relationship between elevated ceramide and depressed S1P levels found during demyelination and the restoration of the disrupted sphingolipid homeostasis during remyelination indicate the potential of modulating these sphingolipid pathways for therapeutic gains. Generally viewed as being pro-survival and cell growth, S1P signals either intracellularly or extracellularly by engaging G-protein coupled S1P receptors (S1P1-5) that are differentially expressed in cells and regulate diverse cellular functions. S1P released from astrocytes in response to exogenous stimuli (3, 6) could act on S1P receptors on OLs or astrocytes. For example, S1P induces process retraction, promotes OL survival (29), inhibits progenitor migration (51), and has been implicated in PDGF-induced progenitor mitogenesis (31). Engagement of astroglial S1P receptors leads to proliferation and neurotrophic factor production (6, 63). S1P receptors 1 and 3 have recently been shown to be upregulated in reactive astrocytes in active and chronic inactive MS lesions (58). Since decreased S1P tissue level during demyelination is fully restored in the remyelinating process, delineating the cellular source for the altered S1P and its interacting receptors shall

provide critical insights for CNS myelin repair. In agreement with this, FTY720 (fingolimod), an analogue of S1P and a first-in-class S1P receptor modulator, is highly effective for relapsing and remitting MS (34) and was recently approved for the treatment of MS. Although impaired egress of immune effector cells out of lymphoid organs (45) is considered to be responsible for the beneficial effect of fingolimod in MS, FTY720 readily crosses the blood-brain-barrier and can thus impact directly on CNS parenchymal cells through engagement of specific S1P receptors. In this respect, it was recently shown that FTY720 modulates glial responses and promotes remyelination after lysolecithin-induced demyelination in cerebellar slice cultures (48). Moreover, a most recent study showed that the efficacy of FTY720 in the T-cell mediated EAE demyelinating model is lost in mutant mice where S1P1 is selectively deleted in astrocytes, indicating a key role for astrocytes in the pathogenesis of EAE (13). Based upon these observations and the findings reported here, future testing of the effect of FTY720 on remyelination and sphingolipid metabolism in the cuprizone model of demyelination is warranted.

In summary, this study identifies aberrant astroglial accumulation of ceramides in human MS and PVL and in animal models of demyelination, and demonstrates, for the first time, reversible changes of specific sphingolipid metabolites such as ceramide, Sph, and S1P during active demyelination and remyelination. We further demonstrate that ceramides markedly promote oligodendroglial cell death in an astrocyte-dependent manner and through, at least in part, acting directly on astrocytes. Our data suggest a previous unrecognized role for ceramide-laden reactive astrocytes in promoting oligodendroglial cell death. Astrocytes could thus represent a potential drug target for modulation of sphingolipid signaling pathways in central white matter injury.

Supplementary Material

Refer to Web version on PubMed Central for supplementary material.

Acknowledgements

This study was funded by NIH grant R01NS060017, grant RG3975 from the National Multiple Sclerosis Society, and by the start-up funds from Texas A&M University. Adult human tissue specimens were kindly provided by the Rocky Mountain MS Center (supported by the National Multiple Sclerosis Society) and the Human Brain and Spinal Fluid Resource Center of the VA West Los Angeles Healthcare Center (sponsored by NINDS/NIMH, National Multiple Sclerosis Society and Department of Veterans Affairs). We are most grateful to Dr. Jacek Bielawski for mass spectrometry measurements of sphingolipids.

References

1. Akassoglou K, Douni E, Bauer J, Lassmann H, Kollias G, Probert L. Exclusive tumor necrosis factor (TNF) signaling by the p75TNF receptor triggers inflammatory ischemia in the CNS of transgenic mice. Proc Natl Acad Sci U S A. 2003; 100(2):709–14. [PubMed: 12522266]
2. Alewijnse AE, Peters SLM, Michel MC. Cardiovascular effects of sphingosine-1-phosphate and other sphingomyelin metabolites. British Journal of Pharmacology. 2004; 143(6):666–84. [PubMed: 15504747]
3. Anelli V, Bassi R, Tettamanti G, Viani P, Riboni L. Extracellular release of newly synthesized sphingosine-1-phosphate by cerebellar granule cells and astrocytes. J Neurochem. 2005; 92(5): 1204–15. [PubMed: 15715670]

4. Antony JM, Ellestad KK, Hammond R, Imaizumi K, Mallet F, Warren KG, Power C. The Human Endogenous Retrovirus Envelope Glycoprotein, Syncytin-1, Regulates Neuroinflammation and Its Receptor Expression in Multiple Sclerosis: A Role for Endoplasmic Reticulum Chaperones in Astrocytes. J Immunol. 2007; 179(2):1210–24. [PubMed: 17617614]
5. Antony JM, van Marle G, Opii W, Butterfield DA, Mallet F, Yong VW, Wallace JL, Deacon RM, Warren K, Power C. Human endogenous retrovirus glycoprotein-mediated induction of redox reactants causes oligodendrocyte death and demyelination. Nat Neurosci. 2004; 7(10):1088–95. [PubMed: 15452578]
6. Bassi R, Anelli V, Giussani P, Tettamanti G, Viani P, Riboni L. Sphingosine-1-phosphate is released by cerebellar astrocytes in response to bFGF and induces astrocyte proliferation through Gi-protein-coupled receptors. Glia. 2006; 53(6):621–30. [PubMed: 16470810]
7. Bezzi P, Domercq M, Brambilla L, Galli R, Schols D, De Clercq E, Vescovi A, Bagetta G, Kollias G, Meldolesi J, Volterra A. CXCR4-activated astrocyte glutamate release via TNFalpha: amplification by microglia triggers neurotoxicity. Nat Neurosci. 2001; 4(7):702–10. [PubMed: 11426226]
8. Bielawski J, Pierce JS, Snider J, Rembiesa B, Szulc ZM, Bielawska A. Comprehensive Quantitative Analysis of Bioactive Sphingolipids by High-Performance Liquid Chromatography–Tandem Mass Spectrometry. Methods in Molecular Biology. 2009; 579:443–67. [PubMed: 19763489]
9. Brody BA, Kinney HC, Kloman AS, Gilles FH. Sequence of Central Nervous System Myelination in Human Infancy. I. An Autopsy Study of Myelination. J Neuropathol Exp Neurol. 1987; 46(3): 283–301. [PubMed: 3559630]
10. Butts BD, Houde C, Mehmet H. Maturation-dependent sensitivity of oligodendrocyte lineage cells to apoptosis: implications for normal development and disease. Cell Death Differ. 2008; 15(7): 1178–86. [PubMed: 18483490]
11. Casaccia-Bonnefil P, Aibel L, Chao MV. Central glial and neuronal populations display differential sensitivity to ceramide-dependent cell death. J Neurosci Res. 1996; 43(3):382–9. [PubMed: 8714527]
12. Chatelut M, Leruth M, Harzer K, Dagan A, Marchesini S, Gatt S, Salvayre R, Courtoy P, Levade T. Natural ceramide is unable to escape the lysosome, in contrast to a fluorescent analogue. FEBS Lett. 1998; 426(1):102–6. [PubMed: 9598987]
13. Choi JW, Gardell SE, Herr DR, Rivera R, Lee C-W, Noguchi K, Teo ST, Yung YC, Lu M, Kennedy G, Chun J. FTY720 (fingolimod) efficacy in an animal model of multiple sclerosis requires astrocyte sphingosine 1-phosphate receptor 1 (S1P1) modulation. Proceedings of the National Academy of Sciences. 2011; 108(2):751–6.
14. Cowart LA, Szulc Z, Bielawska A, Hannun YA. Structural determinants of sphingolipid recognition by commercially available anti-ceramide antibodies. J Lipid Res. 2002; 43(12):2042–8. [PubMed: 12454264]
15. Cutler RG, Kelly J, Storie K, Pedersen WA, Tammara A, Hatanpaa K, Troncoso JC, Mattson MP. Involvement of oxidative stress-induced abnormalities in ceramide and cholesterol metabolism in brain aging and Alzheimer's disease. Proc Natl Acad Sci U S A. 2004; 101(7):2070–5. [PubMed: 14970312]
16. Cutler RG, Pedersen WA, Camandola S, Rothstein JD, Mattson MP. Evidence that accumulation of ceramides and cholesterol esters mediates oxidative stress-induced death of motor neurons in amyotrophic lateral sclerosis. Ann Neurol. 2002; 52(4):448–57. [PubMed: 12325074]
17. El Alwani M, Wu BX, Obeid LM, Hannun YA. Bioactive sphingolipids in the modulation of the inflammatory response. Pharmacol & Ther. 2006; 112(1):171–83. [PubMed: 16759708]
18. Franklin RJM. Why does remyelination fail in multiple sclerosis? Nat Rev Neurosci. 2002; 3(9): 705–14. [PubMed: 12209119]
19. Grassme H, Jendrossek V, Bock J, Riehle A, Gulbins E. Ceramide-rich membrane rafts mediate CD40 clustering. J Immunol. 2002; 168(1):298–307. [PubMed: 11751974]
20. Guan XL, He X, Ong W-Y, Yeo WK, Shui G, Wenk MR. Non-targeted profiling of lipids during kainate-induced neuronal injury. FASEB J. 2006; 20(8):1152–61. [PubMed: 16770014]

21. Han X, Holtzman D, McKeel D, Kelley J, Morris JC. Substantial sulfatide deficiency and ceramide elevation in very early Alzheimer's disease: potential role in disease pathogenesis. J Neurochem. 2002; 82(4):809–18. M. W. [PubMed: 12358786]
22. Hannun YA, Obeid LM. Principles of bioactive lipid signalling: lessons from sphingolipids. Nat Rev Mol Cell Biol. 2008; 9(2):139–50. [PubMed: 18216770]
23. Haughey NJ, Cutler RG, Tamara A, McArthur JC, Vargas DL, Pardo CA, Turchan J, Nath A, Mattson MP. Perturbation of sphingolipid metabolism and ceramide production in HIV-dementia. Ann Neurol. 2004; 55(2):257–67. [PubMed: 14755730]
24. Haynes RL, Baud O, Li J, Kinney HC, Volpe JJ, Folkerth DR. Oxidative and nitrative injury in periventricular leukomalacia: a review. Brain Pathol. 2005; 15(3):225–33. [PubMed: 16196389]
25. Haynes RL, Billiards SS, Borenstein NS, Volpe JJ, Kinney HC. Diffuse axonal injury in periventricular leukomalacia as determined by apoptotic marker fractin. Pediatr Res. 2008; 63(6): 656–61. [PubMed: 18520330]
26. Haynes RL, Folkerth RD, Keefe RJ, Sung I, Swzeda LI, Rosenberg PA, Volpe JJ, Kinney HC. Nitrosative and oxidative injury to premyelinating oligodendrocytes in periventricular leukomalacia. J Neuropathol Exp Neurol. 2003; 62(5):441–50. [PubMed: 12769184]
27. He X, Guan X-L, Ong W-Y, Farooqui AA, Wenk MR. Expression, activity, and role of serine palmitoyltransferase in the rat hippocampus after kainate injury. J Neurosci Res. 2007; 85(2):423–32. [PubMed: 17086544]
28. Ilieva H, Polymenidou M, Cleveland DW. Non-cell autonomous toxicity in neurodegenerative disorders: ALS and beyond. J Cell Biol. 2009; 187(6):761–72. [PubMed: 19951898]
29. Jaillard C, Harrison S, Stankoff B, Aigrot MS, Calver AR, Duddy G, Walsh FS, Pangalos MN, Arimura N, Kaibuchi K, Zalc B, Lubetzki C. Edg8/S1P5: An Oligodendroglial Receptor with Dual Function on Process Retraction and Cell Survival. J Neurosci. 2005; 25(6):1459–69. [PubMed: 15703400]
30. Jana A, Hogan EL, Pahan K. Ceramide and neurodegeneration: Susceptibility of neurons and oligodendrocytes to cell damage and death. Journal of the Neurological Sciences. 2009; 278(1-2): 5–15. [PubMed: 19147160]
31. Jung CG, Kim HJ, Miron VE, Cook S, Kennedy TE, Foster CA, Antel JP, Soliven B. Functional consequences of S1P receptor modulation in rat oligodendroglial lineage cells. Glia. 2007; 55(16): 1656–67. [PubMed: 17876806]
32. Kalyvas A, David S. Cytosolic phospholipase A2 plays a key role in the pathogenesis of multiple sclerosis-like disease. Neuron. 2004; 41(3):323–35. [PubMed: 14766173]
33. Kang Z, Altuntas CZ, Gulen MF, Liu C, Giltiay N, Qin H, Liu L, Qian W, Ransohoff RM, Bergmann C, Stohlman S, Tuohy VK, Li X. Astrocyte-Restricted Ablation of Interleukin-17-Induced Act1-Mediated Signaling Ameliorates Autoimmune Encephalomyelitis. Immunity. 2010; 32(3):414–25. [PubMed: 20303295]
34. Kappos L, Radue E-W, O'Connor P, Polman C, Hohlfeld R, Calabresi P, Selmaj K, Agoropoulou C, Leyk M, Zhang-Auberson L, Burtin P. A Placebo-Controlled Trial of Oral Fingolimod in Relapsing Multiple Sclerosis. N Engl J Med. 2010; 362(5):387–401. [PubMed: 20089952]
35. Kim S, Steelman AJ, Koito H, Li J. Astrocytes promote TNF-mediated toxicity to oligodendrocyte precursors. Journal of Neurochemistry. 2011; 116(1):53–66. [PubMed: 21044081]
36. Kinney HC, Brody BA, Kloman AS, Gilles FH. Sequence of Central Nervous System Myelination in Human Infancy. II. Patterns of Myelination in Autopsied Infants. J Neuropathol Exp Neurol. 1988; 47(3):217–34. [PubMed: 3367155]
37. Kolesnick R, Golde DW. The sphingomyelin pathway in tumor necrosis factor and interleukin-1 signaling. Cell. 1994; 77(3):325–8. [PubMed: 8181053]
38. Kolter T, Sandhoff K. Sphingolipid metabolism diseases. Biochimica et Biophysica Acta (BBA) - Biomembranes. 2006; 1758(12):2057–79.
39. Lassmann, H. Cellular damages and repair in multiple sclerosis. Elsevier Academic Press; 2004.
40. Li J, Baud O, Vartanian T, Volpe JJ, Rosenberg PA. Peroxynitrite generated by inducible nitric oxide synthase and NADPH oxidase mediates microglial toxicity to oligodendrocytes. Proc Natl Acad Sci U S A. 2005; 102(28):9936–41. [PubMed: 15998743]

41. Li J, Ramenaden ER, Peng J, Koito H, Volpe JJ, Rosenberg PA. Tumor necrosis factor {alpha} mediates lipopolysaccharide-induced microglial toxicity to developing oligodendrocytes when astrocytes are present. J Neurosci. 2008; 28(20):5321–30. [PubMed: 18480288]

42. Li X, Becker KA, Zhang Y. Ceramide in redox signaling and cardiovascular diseases. Cell Physiol Biochem. 2010; 26(1):41–8. [PubMed: 20502003]

43. Lucchinetti C, Bruck W, Parisi J, Scheithauer B, Rodriguez M, Lassmann H. Heterogeneity of multiple sclerosis lesions: implications for the pathogenesis of demyelination. Ann Neurol. 2000; 47(6):707–17. [PubMed: 10852536]

44. Mason JL, Toews A, Hostettler JD, Morell P, Suzuki K, Goldman JE, Matsushima GK. Oligodendrocytes and Progenitors Become Progressively Depleted within Chronically Demyelinated Lesions. Am J Pathol. 2004; 164(5):1673–82. [PubMed: 15111314]

45. Matloubian M, Lo CG, Cinamon G, Lesneski MJ, Xu Y, Brinkmann V, Allende ML, Proia RL, Cyster JG. Lymphocyte egress from thymus and peripheral lymphoid organs is dependent on S1P receptor 1. Nature. 2004; 427(6972):355–60. [PubMed: 14737169]

46. Matsushima GK, Morell P. The Neurotoxicant, Cuprizone, as a Model to Study Demyelination and Remyelination in the Central Nervous System. Brain Pathol. 2001; 11(1):107–16. [PubMed: 11145196]

47. Memon RA, Holleran WM, Moser AH, Seki T, Uchida Y, Fuller J, Shigenaga JK, Grunfeld C, Feingold KR. Endotoxin and cytokines increase hepatic sphingolipid biosynthesis and produce lipoproteins enriched in ceramides and sphingomyelin. Arterioscler Thromb Vasc Biol. 1998; 18(8):1257–65. [PubMed: 9714132]

48. Miron VE, Ludwin SK, Darlington PJ, Jarjour AA, Soliven B, Kennedy TE, Antel JP. Fingolimod (FTY720) Enhances Remyelination Following Demyelination of Organotypic Cerebellar Slices. Am J Pathol. 2010; 176(6):2682–94. [PubMed: 20413685]

49. Muscoli C, Doyle T, Dagostino C, Bryant L, Chen Z, Watkins LR, Ryerse J, Bieberich E, Neumman W, Salvemini D. Counter-Regulation of Opioid Analgesia by Glial-Derived Bioactive Sphingolipids. J Neurosci. 2010; 30(46):15400–8. [PubMed: 21084596]

50. Norman JH, Roy GC, Anita T, Justin CM, Diana LV, Carlos AP, Jadwiga T, Avindra N, Mark PM. Perturbation of sphingolipid metabolism and ceramide production in HIV-dementia. Ann Neurol. 2004; 55(2):257–67. [PubMed: 14755730]

51. Novgorodov AS, El-Alwani M, Bielawski J, Obeid LM, Gudz TI. Activation of sphingosine-1-phosphate receptor S1P5 inhibits oligodendrocyte progenitor migration. FASEB J. 2007; 21:1503–14. [PubMed: 17255471]

52. Novgorodov SA, Gudz TI. Ceramide and mitochondria in ischemia/reperfusion. J Cardiovasc Pharmacol. 2009; 53(3):198–208. [PubMed: 19247196]

53. Qin J, Berdyshev E, Goya J, Natarajan V, Dawson G. Neurons and oligodendrocytes recycle sphingosine-1-phosphate to ceramide; significance for apoptosis and multiple sclerosis. J Biol Chem. 2010; 285:14134–43. [PubMed: 20215115]

54. Scurlock K, Dawson G. Differential responses of oligodendrocytes to tumor necrosis factor and other pro-apoptotic agents: Role of ceramide in apoptosis. J Neurosci Res. 1999; 55(4):514–22. [PubMed: 10723061]

55. Spiegel S, Milstien S. Sphingosine-1-phosphate: an enigmatic signalling lipid. Nat Rev Mol Cell Biol. 2003; 4(5):397–407. [PubMed: 12728273]

56. Storch MK, Stefferl A, Brehm U, Weissert R, Wallstrom E, Kerschensteiner M, Olsson T, Linington C, Lassmann H. Autoimmunity to myelin oligodendrocyte glycoprotein in rats mimics the spectrum of multiple sclerosis pathology. Brain Pathol. 1998; 8(4):681–94. [PubMed: 9804377]

57. Trapp BD, Bo L, Mork S, Chang A. Pathogenesis of tissue injury in MS lesions. J Neuroimmunol. 1999; 98(1):49–56. [PubMed: 10426362]

58. Van Doorn R, Van Horssen J, Verzijl D, Witte M, Ronken E, Van Het Hof B, Lakeman K, Dijkstra CD, Van Der Valk P, Reijerkerk A, Alewijnse AE, Peters SL, De Vries HE. Sphingosine 1-phosphate receptor 1 and 3 are upregulated in multiple sclerosis lesions. Glia. 2010; 58(12):1465–76. [PubMed: 20648639]

59. Vielhaber G, Brade L, Lindner B, Pfeiffer S, Wepf R, Hintze U, Wittern K-P, Brade H. Mouse anti-ceramide antiserum: a specific tool for the detection of endogenous ceramide. Glycobiology. 2001; 11(6):451–7. [PubMed: 11445550]

60. Volpe, JJ. Neurology of the newborn. 4th. Philadelphia; Saunders: 2001.

61. Wang G, Silva J, Krishnamurthy K, Tran E, Condie BG, Bieberich E. Direct Binding to Ceramide Activates Protein Kinase C{zeta} before the Formation of a Pro-apoptotic Complex with PAR-4 in Differentiating Stem Cells. J Biol Chem. 2005; 280(28):26415–24. [PubMed: 15901738]

62. Xu Y-H, Barnes S, Sun Y, Grabowski GA. Multi-system disorders of glycosphingolipid and ganglioside metabolism. J Lipid Res. 2010; 51(7):1643–75. [PubMed: 20211931]

63. Yamagata K, Tagami M, Torii Y, Takenaga F, Tsumagari S, Itoh S, Yamori Y, Nara Y. Sphingosine 1-phosphate induces the production of glial cell line-derived neurotrophic factor and cellular proliferation in astrocytes. Glia. 2003; 41(2):199–206. [PubMed: 12509810]

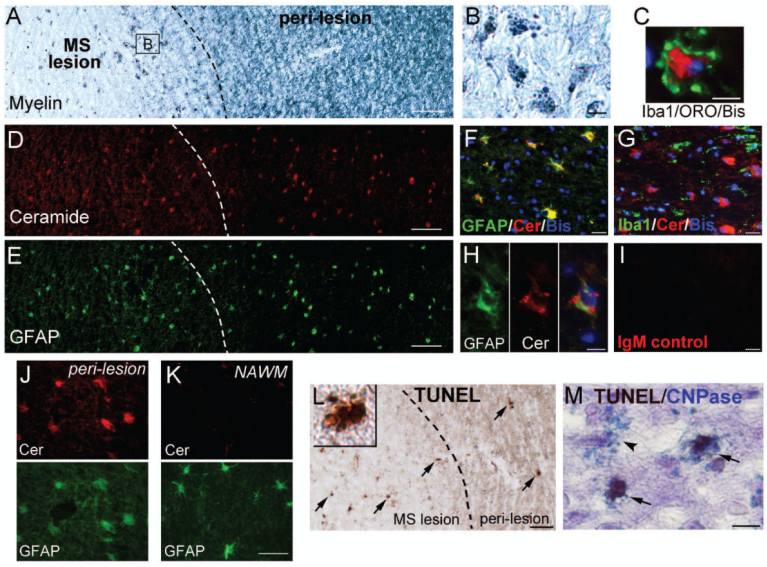

Figure 1. Aberrant accumulation of ceramide in reactive astrocytes in demyelinating lesions of human MS

A, A representative image of actively demyelinating lesions of autopsy MS brains stained for myelin with Sudan black. Myelin debris (***B***) is evident at the lesion edge. ***C***, Microglia/macrophages phagocytosing myelin debris at the edge of active MS lesions. Microglia/macrophages are identified by Iba1 staining (green). Myelin is visualized by oil red O (ORO) staining, and nuclei by bisbenzimide (Bis, blue). ***D-E,*** Double staining of the same brain section with antibodies specific for ceramide (red) and GFAP (green) shows strong ceramide signal in reactive astrocytes in and peri-active MS lesions. The ceramide immunoreactivity is localized to $GFAP^+$ astrocytes (***F***) but not to $Iba1^+$ microglia/macrophages (***G***), and exhibits punctuate staining pattern (***H***). Immunostaining of serial sections with isotype control antibody is negative (***I***). ***J-K,*** Significant ceramide immunoreactivity in reactive astrocytes surrounding demyelinating lesions but not in normal appearing white matter (NAWM) of the same cases. Representative micrographs of double immunostained sections are shown. ***L-M,*** Serial sections stained for TUNEL (***L***, arrows) or double stained for TUNEL (brown) and OL marker CNPase (blue) (***M***), showing damaged OLs (arrows) at the border of the active MS lesion. Arrowhead indicates a $TUNEL^-$/$CNPase^+$ OL (*M*). Scale bars, ***A, D, E***, 100 μm; ***B, C, H***, 10 μm; ***F, G, I,*** 20 μm; ***J-M***, 50 μm.

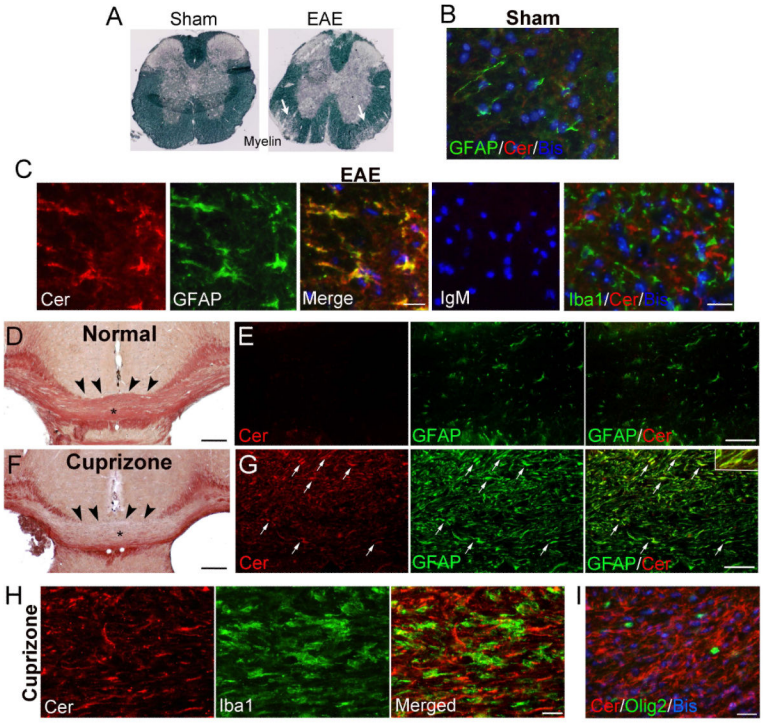

Figure 2. Accumulation of ceramide in reactive astrocytes in animal models of demyelination

A, Representative coronal sections of spinal cords from sham and EAE mice stained with Sudan black. Arrows indicate demyelinating white matter**.** ***B-C,*** Serial spinal cord sections stained for ceramide, GFAP, Iba1, or isotype control antibodies. Ceramide is localized to reactive astrocytes in the spinal cord white matter of EAE but not control mice. Data are representative of 3 animals per group. ***D-I,*** Representative images of ORO- (***D, F***) and immunostained sections (***E, G-I***) showing that cuprizone intoxication induces extensive demyelination in the corpus callosum and marked upregulation of ceramide in reactive astrocytes (arrows in ***G***). Ceramide immunoreactivity is not localized to microglia/macrophages (***H***) and appears not in $Olig2^{+}$ OLs (***I***). Asterisks indicate the immunostained regions in ***E*** and ***G***. Data are representative of 3 control and 5 cuprizone mice. Scale bars, ***B, C,*** 10 μm; ***D, F***, 200 μm; ***E, G***, 50 μm; ***H, I***, 20 μm

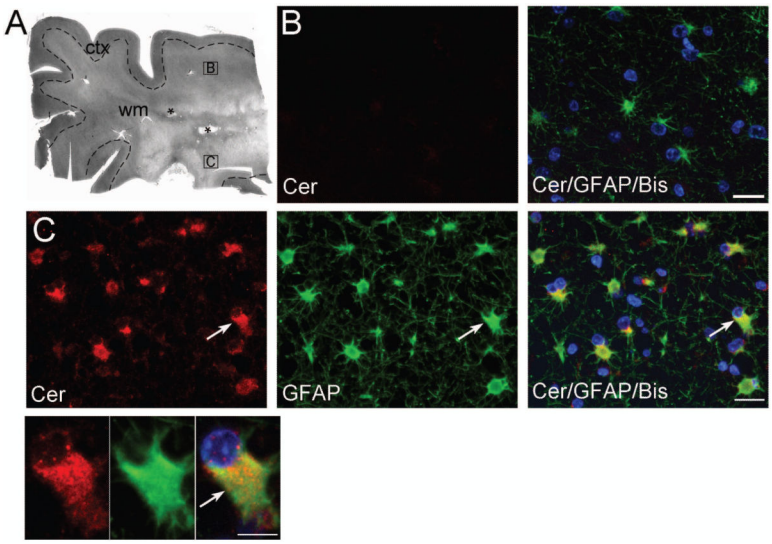

Figure 3. Ceramide is upregulated in reactive astrocytes throughout diffuse white matter lesions of human PVL

A-B, Representative H&E micrograph of a typical PVL with microcysts of focally necrotic lesions (asterisks) in the deep cerebral white matter (wm) of a premature infant born at 35 gestational wk and died at 4 postnatal wk (case #4). Representative areas shown in B-C are depicted here. Reactive astrocytosis is prominent throughout the deep and central white matter distant from the focal lesions. ***B-C***, Immunohistochemistry of serial sections reveals marked upregulation of ceramide in $GFAP^+$ astrocytes throughout the diffuse lesion (***C***), but not in white matter regions with limited reactive astrocytosis and immediate below overlying cortex (ctx) (***B***). Representative micrographs of a $Cer^+/GFAP^+$ cell (***C***, arrow) at a higher magnification are shown on the bottom left. Scale bars, ***B, C***, 20 μm; higher magnification panel in ***C***, 5 μm.

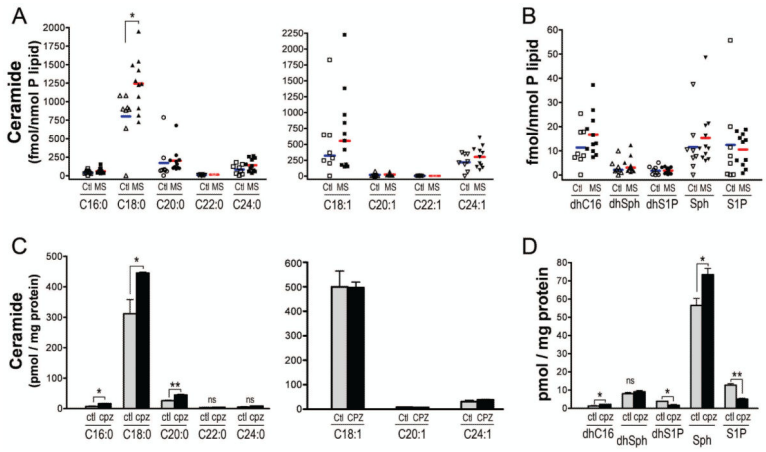

Figure 4. Specific ceramide species are elevated during active demyelination in MS and in animal model of demyelination

A-B, Specific sphingolipids of frozen autopsy human MS and control tissues were analyzed and quantified using HPLC-Tandem Mass Spectrometry. Symbols indicate values from individual cases. C18:0 ceramide is statistically significantly elevated in MS (n=11) as compared to controls (n=8). ***C-D,*** During cuprizone-induced demyelination, C16:0, C18:0 and C20:0 ceramides are significantly upregulated in the cerebral white matter of cuprizone-fed mice. dhC16 and Sph are also significantly elevated in cuprizone-fed mice, whereas the level of dhSph and S1P is significantly decreased during demyelination (n=3 animals per group). *, $p<0.05$; **, $p<0.01$; ns, not significant.

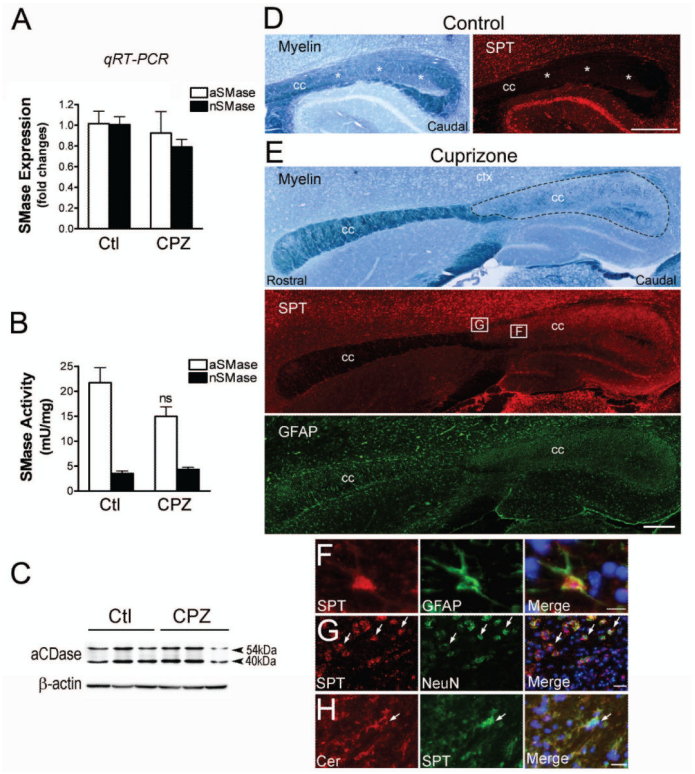

Figure 5. Upregulation of serine palmitoyltransferase in reactive astrocytes during demyelination

A, Quantitative RT-PCR analysis of mRNA expression of acidic and neutral SMase in dissected brains of control and cuprizone-fed mice. No significant changes in SMase transcripts between the two groups (n=3 animals per group). ***B,*** Cerebral acidic and neural SMase enzymatic activities do not differ significantly between control and cuprizone-fed mice. ***C,*** Western blotting analysis of acidic ceramidase (aCDase) expression in dissected brain tissues from control and cuprizone-fed mice. Each lane represents one animal (n=3 animals per group). ***D,*** Representative images of sagittal brain sections of control mice stained for myelin and SPT. SPT expression is minimal in the corpus callosum (cc, asterisks). ***E-F,*** Representative images of Sudan black stained sagittal brain sections of cuprizone-fed mice, showing extensive demyelination in the caudal region of corpus callosum. Double immunostaining shows markedly increased SPT expression in reactive astrocytes in the caudal corpus callosum. Neurons express high level of SPT in both cuprizone-fed mice (***G***, arrows) and controls (***D***). ***H***, Representative image showing colocalization of SPT and ceramide cells in the caudal corpus callosum of cuprizone fed mice. Scale bars, ***D, E***, 500 μm; ***F***, 10 μm; ***G, H***, 20 μm.

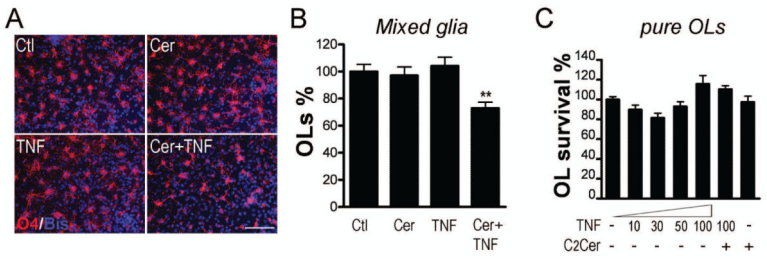

Figure 6. Ceramide promotes oligodendroglial cell death in mixed glial cultures but not in pure cultures

A-B, Cell permeable C2-ceramide (Cer) and TNF synergistically induce significant OL cell loss in mixed glial cultures. Mixed glia were treated with C2-Cer (20 μM), TNF (10 ng/ml) or both as indicated for 48 hr and OL survival was quantified. ***C,*** In highly enriched OL monocultures, TNF (10-100 ng/ml) and C2-ceramide, either alone or in combination, do not cause significant cell death. Data represent three to four independent experiments. **, $p<0.01$.

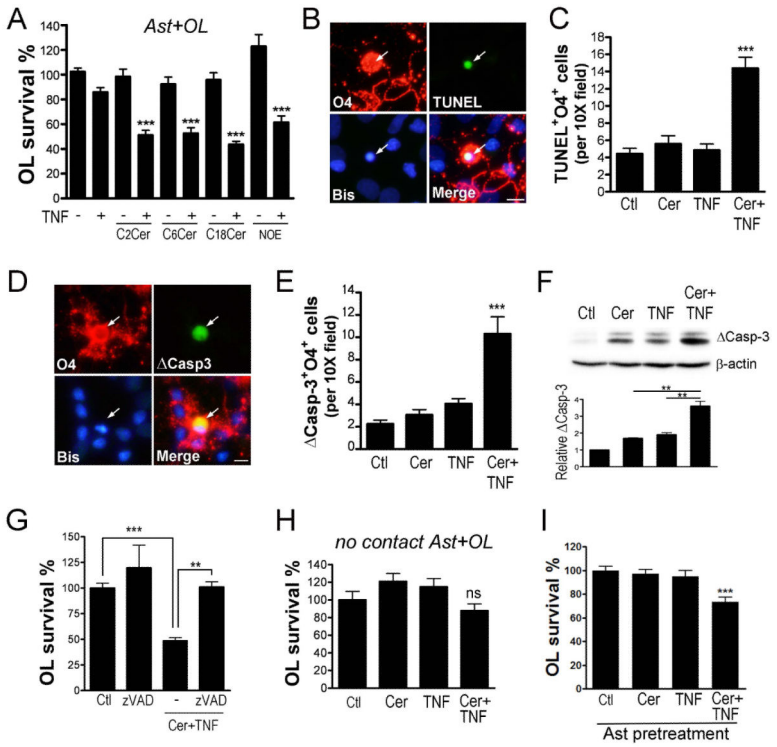

Figure 7. Ceramide potentiates TNF-induced apoptotic death of OLs in an astrocyte-dependent manner

A-B, C2-, C6-, and C18-ceramides (20 μM) act synergistically with TNF (1-5 ng/ml) in astrocytes and OL co-cultures, causing significant cell death. Blocking endogenous ceramide degradation with ceramidase inhibitor NOE also potentiates TNF toxicity. ***, $p<0.001$ when compared to control or corresponding drug treatment in the absence of TNF. ***B-E,*** Representative immunocytochemistry and quantification of $TUNEL^+$ and activated caspase-3 $(\Delta casp3)^+$ OLs in co-cultures of astrocytes and OLs treated with or without C2 ceramide or TNF as indicated. ***, $p<0.001$ when compared to controls. ***F,*** Western blotting analysis for activated caspase-3 in co-cultures treated as indicated. Quantification of Δcasp3 represents two independent experiments. **, $p<0.01$. ***G,*** Caspase inhibitor zVAD-fmk abolished Cer/TNF-induced OL death in co-cultures. ***H,*** The synergistic pro-death effect between TNF and ceramide is abolished if astrocytes and OLs are cultured in two closely opposed layers without direct cell contact. ***I,*** Astrocytes pretreated with C2 ceramide and TNF are subsequently toxic to seeded OLs. Data represent three independent experiments. **, $p<0.01$; ***, $p<0.001$. ns, not significant. Scale bars, ***B, D,*** 10 μm.

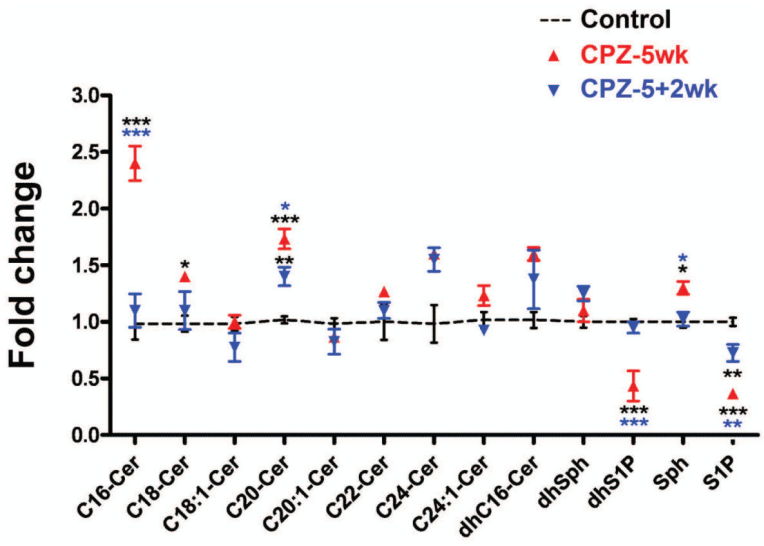

Figure 8. Upregulation of ceramide and loss of S1P during demyelination are significantly reversed during active remyelination in the cuprizone animal model

Comparison of sphingolipid levels in dissected brains from control mice (n=6), mice fed cuprizone for 5 wk (CPZ-5wk, n=3), and mice fed cuprizone for 5wk followed by 2 wk of recovery that results in efficient remyelination (CPZ-5+2 wk, n=4). Ceramides that are significantly elevated in CPZ 5wk mice are significantly decreased in CPZ 5+2wk mice. Loss of S1P and dhS1P during demyelination are also recovered in 5+2 wk mice. Data represent mean ± sem. Black asterisks, when compared with control; blue asterisks, when CPZ 5wk compared with 5+2wk. *, $p<0.05$; **, $p<0.01$; ***, $p<0.001$.

Table 1

Summary of clinicopathologic information and neuropathologic findings on MS and control cases

Diagnosis	Case No.	Age/Sex	Clinical diagnoses or cause of death	Microscopic Classification*	Ceramide signals in astrocytes†
Control	**C-#1**	86/F	nk	−	−
	C-#2	62/F	Lewy body disease, Dementia	−	+
	C-#3	74/M	Progressive Supranuclear Palsy	−	−
	C-#4	?/M	Respiratory failure, sepsis	−	−
	C-#5	19/M	Gun shot (chest/abdomen)	−	−
	C-#6	15/M	Normal, accidental hanging	−	−
	C-#7	31/M	Anemia, pancytopenia, obesity	−	+
	C-#8	29/M	Normal, motor cycle accident	−	+
MS	**MS-#1**	69/M	MS	**Infl. − /Demyel. −**	++
	MS-#2	44/M	MS (chronic progressive), aspiration pneumonia, grand mal seizure with status epilepticus	**Infl. + /Demyel. +**	−
	MS-#3	40/F	MS (progressive, severe, unrelenting ~10 yrs)	**Infl. + /Demyel. +**	+++
	MS-#4	43/F	MS (chronic progressive)	**Infl. − /Demyel. −**	+
	MS-#5	42/M	MS (type unavailable, ~10 yrs), suicide	**Infl. + /Demyel. +**	++
	MS-#6	33/M	MS (chronic progressive)	**Infl. + /Demyel. +**	+++
	MS-#7	49/F	MS (type and duration unknown)	**Infl. Rim + /Demyel. +**	++
	MS-#8	63/F	MS, sleep apnea, chronic urinary tract infection, respiratory failure, hypertension	**Infl. Rim +/Demyel. +**	−
	MS-#9	52/F	MS (2nd progressive), chronic urinary tract infection, respiratory failure	**Infl. Rim +/Demyel.+**	+
	MS-#10	51/F	MS (2nd progressive), depression	**Infl. Rim +/Demyel. +**	++
	MS-#11	75/F	MS, hypertension, kidney stone surgery, goiter surgery, hypothyroidism, migraine, chronic urinary tract infection	**Infl. − /Demyel. −**	+++
	MS-#12	59/M	MS (primary progressive), dementia, tobacco abuse	**Infl. + /Demyel. −**	−
	MS-#13	54/F	MS (relapse/remitting)	**Infl. Rim + /Demyel. +**	+++

M=male, F=female, nk=not known

*Microscopic classification was based on the Vienna consensus for MS lesion staging/description (56). Infl.+ (inflammatory): denote the presence of inflammatory cells (including macrophages) Demyel.+ (demyelinating): denote the presence of recognizable myelin breakdown products in macrophages Infl. Rim+: denote the presence of inflammatory rim (and hypocellular centre).

†Based on double immunohistochemistry. Immunofluorescence signal was analyzed by two independent investigators and the intensity of ceramide immunoreactivity in $GFAP^+$ cells in relation to background signal (unaffected white matter areas of the same tissue section) was semi-scored in scale of: −, minimum; +, weak; ++, moderate; +++, strong.

Table 2

Summary of the clinicopathologic information and neuropathologic findings on PVL and control cases

Diagnosis	Case # /sex	GA (wk)*	PA (wk)	PCA (wk)**	Other clinicopathologic data	Microglia activation†	Ceramide signal in AST‡
Control	**1/M**	33	1	34	Tracheoesophageal fistula, small ventricular septal defect, respiratory distress, prematurity	−	−
	2/M	32	2	34	Bradycardia, cyanotic, prematurity, comfort care	+	−
	3/M	39	1	40	Nodular cortical dysplasia, focal pontosubicular necrosis, liver function abnormalities	++	−
PVL	**PVL #1/F**	31	2	33	Congenital heart defect, prematurity, sepsis, prematurity	−	−
	PVL #2/F	32	1	33	Intraventricular hemorrhage, septic shock, prematurity	+	+
	PVL #3/F	34	4	38	Congenital diaphragmatic hernia, prematurity	+	++
	PVL #4/F	35	5	40	Renal failure, diffuse sclerosis, ventilator dependent, prematurity	+++	+++
	PVL #5/M	38	2	40	Primary pulmonary hypertension, cerebral infarct, sepsis	++	+

nk=not known, PA=postnatal age

*GA=Gestational age. The time from conception until birth. More specifically, gestational age is defined as the number of weeks from the first day of the mother's last menstrual period (LMP) until the birth of the baby. Gestational age at birth is assessed by the date of the LMP and by physical exam (Dubowitz score). Mean ± SD of GA: 34.7 ± 3.8 wk (control) and 34.0 ± 2.7 wk (PVL).

**PCA=Post-conceptional age. Age since conception. Post-conceptional age is calculated as gestational age plus postnatal age. Mean ± SD of PCA: 36.0 ± 3.5 wk (control) and 36.8 ± 3.6 wk (PVL).

†Microglia/macrophage activation was determined by $CD68^+$ cells in the cerebral white matter and diffuse component of PVL. Labeling index: Immunoreactive intensity was defined as mild (+), moderate (++), or intense (+++), − indicates no or minimum signal.

‡Based on immunohistochemistry. When ceramide+ cells was counted and scored, necrotic focal lesion regions were excluded and only diffuse lesions were analyzed.